Hybrid Nanomaterials

DOI: 10.1002/ange.201402935

Preparation of MoS_2–MoO_3 Hybrid Nanomaterials for Light-Emitting Diodes**

*Zongyou Yin, Xiao Zhang, Yongqing Cai, Junze Chen, Jen It Wong, Yee-Yan Tay, Jianwei Chai, Jumiati Wu, Zhiyuan Zeng, Bing Zheng, Hui Ying Yang, and Hua Zhang**

Abstract: *A facile strategy to prepare MoS_2–MoO_3 hybrid nanomaterials is developed, based on the heat-assisted partial oxidation of lithium-exfoliated MoS_2 nanosheets in air followed by thermal-annealing-driven crystallization. The obtained MoS_2–MoO_3 hybrid nanomaterial exhibits p-type conductivity. As a proof-of-concept application, an n-type SiC/p-type MoS_2–MoO_3 heterojunction is used as the active layer for light-emitting diodes. The origins of the electroluminescence from the device are theoretically investigated. This facile synthesis and application of hybrid nanomaterials opens up avenues to develop new advanced materials for various functional applications, such as in electrics, optoelectronics, clean energy, and information storage.*

Ultrathin layered MoS_2 nanosheets have been widely studied recently because of their unique physical, electrical, and optical properties.[1] To prepare ultrathin MoS_2 nanosheets, many methods have been developed, which include mechanical exfoliation,[2] solvent exfoliation,[3] lithium intercalation,[4] and chemical vapor deposition.[5] In particular, the characteristics of 2D MoS_2 nanosheets have been intensively investigated. For example, its electrocatalytic activity for hydrogen production has been found to be only slightly lower than that of the precious platinum noble metals and thus surpasses most common metals, which might arise from the large number of active edge-sites on MoS_2.[6] Additionally, as the channel of field-effect transistors (FETs), the single-layer MoS_2-based top-gated FET exhibited ultra-high channel mobility (approximately 200 $cm^2 V^{-1} s^{-1}$) and a current on/off ratio of approximately 10^8.[7] These results enable single-layer MoS_2 to be a competitive candidate for potential replacement of silicon in CMOS-like logic devices (CMOS = complementary metal–oxide semiconductor).[2,3,4b,8] Furthermore, the quantum enhancement in the photoluminescence (PL) intensity from a few layers to a single layer can be measured in both mechanically[9] and chemically[4b] exfoliated MoS_2 nanosheets. Impressively, single-layer MoS_2-based phototransistors with high photoresponsivity[10a,b] and diodes with excellent electroluminescence (EL)[10c,d] have been reported.

As an important class of materials, 2D hybrid nanostructures are attracting intense interest. For instance, the vertically layered heterostructured FETs, that is, graphene/BN/graphene[11] and graphene/WS_2/graphene[12] prepared by the dry-transfer technique, exhibited field-effect vertical-tunneling characteristics. The FETs based on n-MoS_2/graphene and n-MoS_2/graphene/p-$Bi_2Sr_2Co_2O_8$/graphene vertical heterostructures showed the functional properties of logic transistors and complementary inverters.[13] The layered MoS_2/graphene composite, synthesized by the solvothermal method, was used as an anode material for a lithium-ion battery with excellent electrochemical performance.[14] The layered nanojunction of MoS_2/CN, synthesized by wet impregnation followed by thermal-assisted sulfidation, showed excellent photocatalysis for H_2 evolution.[15] Moreover, the Van der Waals heterostructures of WSe_2/MoS_2 were recently studied for exploration of the EL and photocurrent generation properties.[10e]

Herein, we demonstrate a facile method to prepare MoS_2–MoO_3 hybrid nanomaterials. The preparation is achieved through the in situ partial oxidation of MoS_2 nanosheets during their film preparation by a heat-assisted spray-coating procedure in air, followed by thermal-annealing-driven crystallization. After spray coating the obtained $MoS_{2-x}O_x$ film on an arbitrary solid substrate, such as Si, SiC, quartz, or glass, the material undergoes thermal treatment and crystallizes to form MoS_2–MoO_3 hybrid nanomaterials composed of (100)-dominated MoS_2 and (021)-dominated α-MoO_3. The obtained MoS_2–MoO_3 nanomaterial exhibits

[*] Dr. Z. Y. Yin,[+] X. Zhang,[+] J. Z. Chen, Dr. Y. Y. Tay, J. Wu, Dr. Z. Y. Zeng, Dr. B. Zheng, Prof. H. Zhang
School of Materials Science and Engineering
Nanyang Technological University
50 Nanyang Avenue, Singapore 639798 (Singapore)
E-mail: hzhang@ntu.edu.sg
Homepage: http://www.ntu.edu.sg/home/hzhang/
Dr. Y. Q. Cai[+]
Institute of High Performance Computing
A*STAR (Agency for Science, Technology and Research)
1 Fusionopolis Way, Singapore 138632 (Singapore)
Dr. J. W. Chai
Institute of Materials Research and Engineering
A*STAR (Agency for Science, Technology and Research)
3 Research Link, Singapore 117602 (Singapore)
Dr. J. I. Wong, Prof. H. Y. Yang
Pillar of Engineering Product Development
Singapore University of Technology and Design
20 Dover Drive, Singapore 138682 (Singapore)
[+] These authors contributed equally to this work.

[**] This work was supported by MOE under AcRF Tier 2 (ARC 26/13, No. MOE2013-T2-1-034), AcRF Tier 1 (RG 61/12, RGT18/13, and RG5/13), and Start-Up Grant (M4080865.070.706022) in Singapore. This Research is also conducted by NTU-HUJ-BGU Nanomaterials for Energy and Water Management Program under the Campus for Research Excellence and Technological Enterprise (CREATE), that is supported by the National Research Foundation, Prime Minister's Office, Singapore.

Supporting information for this article is available on the WWW under http://dx.doi.org/10.1002/anie.201402935.

p-type conductivity. As a proof-of-concept, a light-emitting diode (LED) is demonstrated, which is based on a heterojunction composed of a p-type MoS_2–MoO_3 (p-MoS_2–MoO_3) film and an n-type 4H-SiC (n-SiC) substrate, and exhibits multi-wavelength emission. Two bands in its EL spectrum are assigned to the internal radiative recombination of electrons from the conduction band (CB) and holes from the valence band (VB) of MoS_2, and that of electrons from the CB and holes from the VB of MoO_3, respectively. The other two bands were correlated to the defect energy levels in MoO_3 supported by theoretical calculations.

In a typical experiment (see Experimental Section for further details), the lithium-exfoliated MoS_2 nanosheets, prepared by our recently developed method,[4a] were first sonicated in a water bath (Figure 1a). Field-emission scanning electron microscopy (FE-SEM) images in Figure 2a show that the lateral size of MoS_2 flakes is approximately 0.2–2 μm. Transmission electron microscopy (TEM) was used to investigate the morphology and structure of the sonicated MoS_2 nanosheets. The TEM images of MoS_2 nanosheets confirm the lattice structure of MoS_2 (Figure S1a,b in the Supporting Information). The thinnest of the MoS_2 nanosheets obtained were approximately 1.8 nm in thickness (Figure 2b, Figure S2a) while some stacked nanosheets were also evident (Figure S2b). Note, sonication of Li-exfoliated MoS_2 had negligible contribution on the oxidation of MoS_2, which can be seen from the X-ray photoelectron spectroscopy (XPS) results for the sonicated and original Li-exfoliated MoS_2 nanosheets (Figure S3).

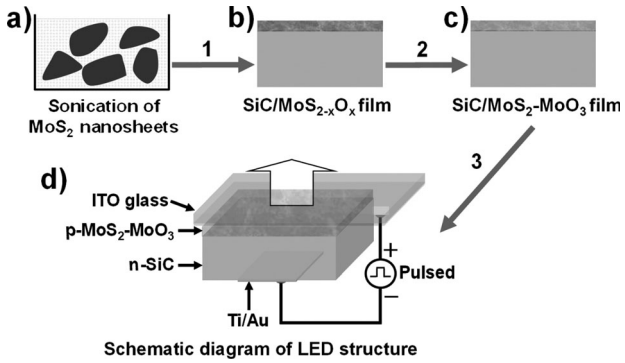

Figure 1. Schematic illustration of the preparation of MoS_2–MoO_3 hybrid nanomaterials used for the LED device: a) Sonication of MoS_2 sheets dispersed in aqueous solution; b) In situ partial oxidization of MoS_2 to $MoS_{2-x}O_k$ by heat-assisted spray-coating of the MoS_2 solution on SiC in air (1); c) SiC/MoS_2–MoO_3 film formed after thermal annealing of the SiC/$MoS_{2-x}O_x$ film (2); d) Configuration of the LED device after fabrication using p-MoS_2–MoO_3 and n-SiC heterojunction as the active layer (3).

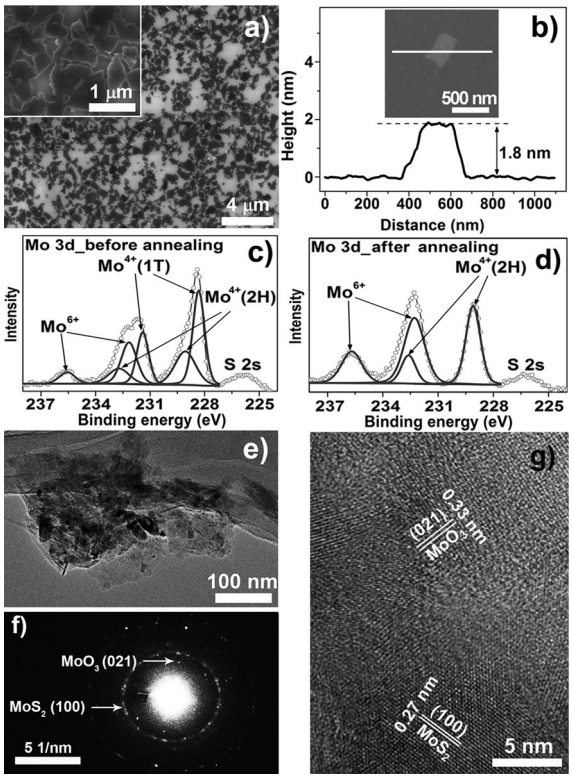

Figure 2. a) SEM image of sonicated MoS_2 nanosheets. Inset: Magnified SEM image. b) Measurement of the thickness of the thinnest MoS_2 nanosheet by AFM. c,d) XPS spectra of (c) $MoS_{2-x}O_x$ before annealing, which was obtained after spray-coating of MoS_2 nanosheets, and (d) MoS_2–MoO_3 hybrid material obtained after thermal annealing of $MoS_{2-x}O_x$. e) TEM image of a fragment scratched from the MoS_2–MoO_3 film. f) SAED pattern taken from the sample in (e). g) HRTEM image with both MoO_3 and MoS_2 components taken from the sample in (e), showing MoO_3 and MoS_2 lattice-fringe spacings.

To prepare MoS_2–MoO_3 hybrid nanomaterials, MoS_2 nanosheets were first partially oxidized to $MoS_{2-x}O_x$ during the spray-coating process in air. The composition of the $MoS_{2-x}O_x$ film on a 4H-SiC substrate (referred to as a SiC/$MoS_{2-x}O_x$ film; Figure 1b) was confirmed by XPS (Figure 2c). Subsequently, the thermal-annealing-induced crystallization of the $MoS_{2-x}O_x$ film was achieved at high temperature, thus forming a SiC/MoS_2–MoO_3 film (Figure 1c). The product, namely the MoS_2–MoO_3 hybrid nanomaterial, was further characterized by XPS (Figure 2d) and TEM (Figure 2e–g).

The XPS results confirmed the coexistence of Mo^{4+} and Mo^{6+} ions in $MoS_{2-x}O_x$ (Figure 2c) and a MoS_2–MoO_3 hybrid material obtained after annealing of $MoS_{2-x}O_x$ (Figure 2d). The two peaks at 232.6 eV (Mo^{4+} $3d_{3/2}$) and 229.1 eV (Mo^{4+} $3d_{5/2}$) in both Figure 2c and Figure 2d are from the semiconducting 2H-phase MoS_2, and those at 235.6 eV (Mo^{6+} $3d_{3/2}$) and 232.2 eV (Mo^{6+} $3d_{5/2}$) are from MoO_3. Note that in Figure 2c, the two peaks located at 231.6 eV (Mo^{4+} $3d_{3/2}$) and 228.3 eV (Mo^{4+} $3d_{5/2}$) are assigned to metallic 1T-phase MoS_2. The slight decrease detected in the binding energy from 2H-phase to 1T-phase MoS_2 was also reported previously.[4b,16] In addition, the coexistence of 1T- and 2H-phase MoS_2 is normally found in the lithium-exfoliated MoS_2, but the 1T-phase can be completely converted into the stable 2H-phase upon annealing above 300 °C.[4b,17] The complete conversion is also confirmed from the XPS result (Figure 2d), where only 2H-phase MoS_2 was evident in the MoS_2–MoO_3 hybrid material. The coexistence of MoS_2 and MoO_3 was also confirmed by energy-dispersive X-ray spectroscopy (EDS)

elemental mapping of both $MoS_{2-x}O_x$ (Figure S4a) and MoS_2–MoO_3 (Figure S4b). The weight ratio of MoO_3 to MoS_2 is approximately 2:3, based on the XPS results in Figure 2d.

The low-magnification TEM image of one MoS_2–MoO_3 fragment is shown in Figure 2e. The selected area electron diffraction (SAED) pattern (Figure 2f) contains signals for both MoS_2 and MoO_3. We can clearly see (021)-indexed diffraction spots for MoO_3 and (100)-indexed diffraction spots for MoS_2 in one SAED pattern. This area was further characterized by high-resolution TEM (HRTEM). In Figure 2g, a lattice fringe with a spacing of 0.33 nm was observed, which is consistent with the theoretical lattice spacing of orthorhombic α-MoO_3 (021) planes.[18] Meanwhile, the typical MoS_2 lattice spacing of 0.27 nm was also observed, which indicates the coexistence of MoS_2 and MoO_3 in the fragment (Figure 2g).

The X-ray diffraction (XRD) data for experiments based on the MoS_2–MoO_3 film (Figure S5) also indicated that the annealing process enables the $MoS_{2-x}O_x$ to crystallize. The crystalline MoS_2–MoO_3 hybrid nanomaterial was confirmed to be formed based on the TEM results (Figure 2e–g). The formation of the nanomaterial was further verified from the XRD patterns, in which a strong (021) peak attributable to MnO_3 at approximately 27.3 degree dominates the spectrum (Figure S5).

A Hall measurement was performed to characterize the doping characteristics of the MoS_2–MoO_3 hybrid film. The film has p-type hole conductivity with a measured doping concentration of 10^{16}–10^{18} cm^{-3}. As a proof-of-concept application, the light-emitting diode (LED) device, with an n-SiC/p-MoS_2–MoO_3 heterojunction as the active layer, was fabricated (see detailed device structure and fabrication in Figure 1d, and Experimental Section). The SEM cross-section image in Figure S6 reveals that the thickness of the prepared MoS_2–MoO_3 film is approximately 3 μm.

Figure 3a shows the current-voltage (*I-V*) curve measured for the prepared LEDs (device structure given in Figure 1d). It can be seen that the LED device exhibits a turn-on voltage of approximately 4.5 V. When the applied forward bias was increased to 10 V, the current reached approximately 15 mA. The inset in Figure 3a shows a lighting photo of the LED device taken at forward bias of 18 V, where we can see the intense light emission from the transparent ITO electrode (ITO = indium tin oxide) of the LED. In combination, the *I-V* characteristics and light emission of the n-SiC/p-MoS_2–MoO_3 heterojunction LED device indicate that the MoS_2–MoO_3 hybrid nanomaterial works efficiently as a p-type hole-injection layer in the device. Figure 3b shows the EL spectra of the LED device biased at different forward voltages. The EL spectra show broad emission profiles with four sub-bands located at $\lambda = 411$, 459, 553, and 647 nm, respectively, after fitting the spectrum taken at 18 V (inset in Figure 3b).

To understand the origins of the peaks detected in the EL spectrum and the p-type hole conductivity associated with defects in the MoS_2–MoO_3 layer, first-principle calculations were performed to investigate the electronic properties and the alignment of energy levels in MoS_2–MoO_3. First, the effect of point defects in MoS_2 was neglected, since the sulfur vacancy, which is one of the most likely defect types in a MoS_2

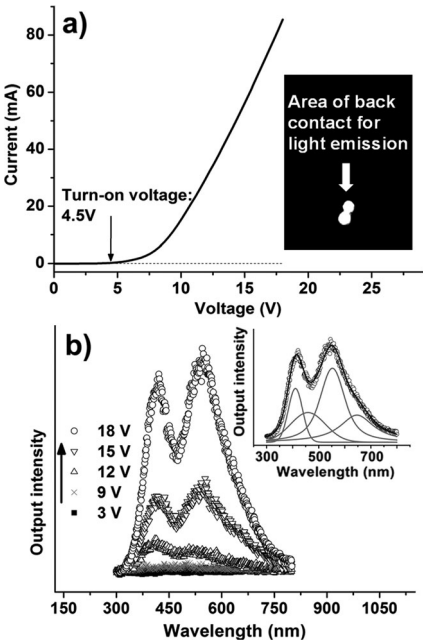

Figure 3. a) Current-voltage (*I-V*) curve of LEDs with device configuration Au/Ti/n-SiC/p-MoS_2–MoO_3/ITO/glass. Inset: Lighting photo of the LED taken at 18 V. b) EL spectra of the LED device biased at different forward voltages. Inset: Fitting of sub-bands for the EL spectrum taken at 18 V.

film, has shown to create deep gap states and is unlikely to give rise to the measured p-type conductivity.[20] Second, the possibility of oxygen substitution of sulfur in MoS_2 is ruled out because there is no defective state in the band gap resulting from the substitution (Figure S7).

We are particularly interested in the defects in MoO_3, which are probably introduced during the oxidation of MoS_2 to form MoO_3. The proposed oxygen-deficient oxide components consist of several intermediate molybdenum oxides, such as Mo^{5+} or Mo^{4+}, which accompany the deep defective state, that is, the oxygen vacancy (V_O), about 1 eV below the CB localized on the neighboring Mo atoms (labeled as D1, Figure 4e).[21] On the other hand, the incomplete oxidation of MoS_2 during thermal treatment is highly possible. As a result, sulfur atoms from MoS_2 can occupy the site for oxygen atoms in MoO_3. These defects may be considered as an S substitution of an O atom (denoted as S_O) in the MoO_3. The α-MoO_3 phase involves three types of oxygen atoms, that is, the singly coordinated oxygen (O1), twofold-coordinated oxygen (O2), and threefold-coordinated oxygen atom (O3). Sulfur substitutions of O1, O2, and O3 atoms are labeled as S_{O1}, S_{O2}, and S_{O3}, respectively (Figure 4a). In contrast to the V_O defect, plots of density of states (DOS) in Figure 4a show that these S_O defects create defective states which are overlapped and located about 0.5 eV above the VB (labelled as D2, Figure 4e). The D2 states of S_{O1}, S_{O2}, and S_{O3} defects are found to have p_x(S)-d_{xy}(Mo), p_yp_z(S)-d_{xz}(Mo), and p_xp_y(S)-d_{xz}(Mo) hybridization, with a p:d orbital occupation ratio of 1:0.40, 1:0.41, and 1:0.29, respectively. These defective states above the VB of MoO_3 play an important role in both producing the p-type carriers and giving rise to the features observed in the

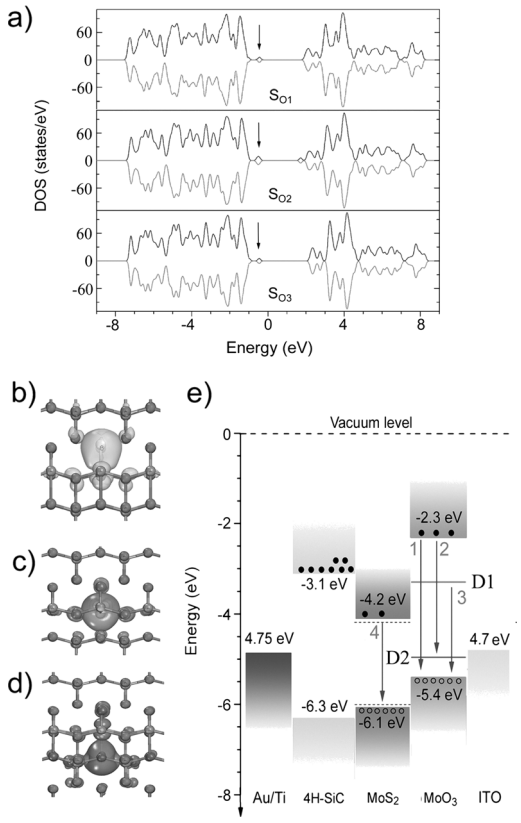

Figure 4. a) DOS of spin-up (black lines) and spin-down (gray lines) electrons in MoO_3 containing S_{O1}, S_{O2}, and S_{O3} defects. The arrows indicate the defective states in the band gap. b–d) Isosurface plots of the charge density of the defective states of S_{O1} (b), S_{O2} (c), and S_{O3} (d). e) Energy diagram for the hybrid systems composed of 4H-SiC, MoS_2, and MoO_3. Electroluminescence transition scheme is plotted. Transition 1 corresponds to the transition from the CB to the VB of MoO_3. Transition 4 corresponds to the recombination of electrons at the CB and holes at the top valence band at the K point of the Brillouin zone of MoS_2, with thickness from a single layer to a few layers. Single layer MoS_2 was used in (e) to illustrate the band gap, where the dashed lines within the band gap represent the slight decrease of the gap with increasing the number of layers of MoS_2. Transition 2 corresponds to the transition from the CB of MoO_3 to the S_{Ox}-related ($x=1$, 2, 3) D2 level, whereas transition 3 is from the V_O-related D1 level to the VB of MoO_3. The work function of Au/Ti (4.75 eV) and ITO (4.7 eV) is taken from Refs. [31a,b]. The electron affinity for 4H-SiC (3.1 eV), MoS_2 (4.2 eV), and MoO_3 (2.3 eV) was obtained from Refs. [31c,d,e].

EL spectrum. Isosurface plots for the defective states are shown in Figure 4b–d, from which the larger component of p states of substituting S atoms compared to the neighboring Mo atom are evident. Note that there are also some contributions from the 2p orbitals of O atoms around the defect center.

The energy-band alignment of the defective MoO_3 and n-type 4H-SiC is shown in Figure 4e. The schematic energy bands of mixed MoS_2 and MoO_3 components were drawn separately for clarity. Under the forward bias, the injected holes at the VB of MoO_3 can partially relax nonradiatively to the D2 level. Then, the holes from D2 can radiatively recombine with injected electrons at the CB of MoO_3, thus producing EL emission bands which are governed by the selection rule ($\Delta l = \pm 1$, for example s–p, p–d transitions). In the EL spectrum, the first emission band, which is detected at $\lambda = 411$ nm (3.02 eV), can be ascribed to the direct recombination of electrons from the CB and holes from the VB in MoO_3. This occurs as the injected electrons from the CB of the SiC substrate can relax to the CBs of MoO_3, and holes can be directly injected onto the VBs of MoO_3. The peak at $\lambda =$ 647 nm (1.92 eV), that is, the fourth emission, arises from the recombination of electrons and holes in the MoS_2 layer. Owing to the applied voltage and weak screening effect in the atomically thin MoS_2 layer, its Fermi level can shift below the valence-band maximum.[19] Therefore, the injected holes from ITO to MoS_2 can accumulate at the top valence band at the K point of the Brillouin zone, which relates to recombination of the A exciton with peak positions which are nearly insensitive to thickness (approximately 1.86–1.89 eV).[4b,9a] With this in mind, we used single-layer MoS_2 in the theoretical calculations for simplicity, as illustrated in Figure 4e. The other two peaks, that is, at $\lambda = 459$ nm (2.7 eV) and $\lambda = 553$ nm (2.24 eV), are related to the radiative recombination of carriers occupying D1 and D2 defective levels in the MoO_3 layer. The emission at $\lambda = 459$ nm arises from the recombination of electrons at the CB with holes at the D2 level in MoO_3, whereas the emission centered at $\lambda = 553$ nm is likely to arise from the transition from the V_O-related D1 level to the VB of MoO_3. As a result of the lattice distortion and defects in the layers, these emission bands are broadened. The experimental data are consistent with the theoretically predicted emission bands from the LED devices (Table 1).

Table 1: Experimental and theoretical EL transitions for n-SiC/p-MoS_2–MoO_3-based LEDs.

Transition	EL peaks (experimental)	EL peaks (theory)
CB (MoO_3) $\rightarrow$VB (MoO_3)	$\lambda = 411$ nm (3.02 eV)	$\lambda = 400$ nm (3.1 eV)
CB (MoO_3) $\rightarrow$D2	$\lambda = 459$ nm (2.7 eV)	$\lambda = 459$ nm (2.7 eV)
D1 $\rightarrow$VB (MoO_3)	$\lambda = 553$ nm (2.24 eV)	$\lambda = 590$ nm (2.1 eV)
CB (MoS_2) $\rightarrow$VB (MoS_2)	$\lambda = 647$ nm (1.92 eV)	$\lambda = 653$ nm (1.9 eV)

Previous studies of MoS_2 have demonstrated the important and effective role of appropriate contacts in tuning the Schottky barriers.[27,28] The addition of a thin oxide barrier, such as MgO[29] and TiO_2,[30] can greatly eliminate the contact resistance and alleviate the conduction mismatch. The ability to tune the height and width of the Schottky barrier by contact engineering opens the possibility to tune the mobility and polarity of conducting carriers. Similarly, the Schottky barrier formed between the MoS_2–MoO_3 hybrid film and the metal contacts tends to be not only determined by the work function, but also affected by the significant interfacial states and defective states. Controlling the Schottky barriers will be very important in potential devices based on MoS_2–MoO_3 hybrid nanomaterials and deserves further detailed exploration.

In conclusion, a facile preparation strategy for MoS_2–MoO_3 hybrid nanomaterials was developed through heat-assisted partial oxidation of MoS_2 nanosheets in air followed by the subsequent thermal-annealing-driven crystallization. The obtained MoS_2–MoO_3 material exhibited p-type conductivity. As a proof-of-concept application, an n-SiC/p-MoS_2–MoO_3 heterojunction was applied in LEDs. The origins of EL peaks from these devices were theoretically explored and it was shown that radiative recombination processes relating to band edges and defect energy levels played key roles. We believe that our facile synthesis of hybrid nanomaterials for functional applications may provide opportunities to develop new advanced 2D hybrid nanomaterials for various applications in optoelectronics, clean energy, and information storage.

Experimental Section

Preparation of MoS_2–MoO_3 hybrid nanomaterials: Molybdenum disulfide (MoS_2, of size 10–30 μm) was purchased from Rose Mill (West Hartford, USA). The detailed electrochemical lithium-intercalation method for preparation of MoS_2 nanosheets was described in our previous report.[4a] Herein, after the lithium-intercalated MoS_2 nanosheets were sonicated in a water bath for 3 h, they were washed with Milli-Q water twice by centrifugation and redispersed in water. The sonicated MoS_2 nanosheets were deposited on a solid substrate, such as Si, SiC, quartz, or glass, by the spray-coating method. During the coating process, the substrate was heated on a hot plate at 90 °C to accelerate the solvent evaporation and increase the oxidation content of MoS_2. Subsequently, the obtained $MoS_{2-x}O_x$ was annealed in 5 % H_2-diluted Ar gas at 450–500 °C for 1 h to crystallize the MoS_2–MoO_3 hybrid nanomaterials. The detailed film preparation and annealing experiments are presented in the device fabrication section (see below), where the SiC substrate was used.

Characterization: Scanning electron microscopy (SEM) was performed using a JEOL JSM-7600F field-emission scanning electron microanalyzer at an accelerating voltage of 5 kV. Elemental distribution mapping based on energy-dispersive X-ray (EDX) spectroscopy was determined with a JEOL JSM-7600F field-emission scanning electron microanalyzer under transmission mode using the transmission electron detector (TED). Atomic force microscopy (AFM) images and thickness measurements were obtained using tapping-mode AFM (Dimension ICON with Nanoscope V controller, Bruker). X-ray photoelectron spectroscopy characterization (XPS, Axis Ultra) was utilized to characterize elemental composition. Transmission electron microscope (TEM), high-resolution TEM (HRTEM), and selected area electron diffraction (SAED) were performed on a JEOL 2100F with a beam energy of 200 keV. X-ray diffraction (XRD) was conducted using a Siemens D-500 X-ray diffractometer (Bruker AXS, Inc., Madison, USA). The Hall effect system (HL5500, Bio-Rad Microscience Limited, UK) was used to measure the doping characteristics of MoS_2–MoO_3 hybrid nanomaterials at room temperature. The thickness of $MoS_{2-x}O_x$ or MoS_2–MoO_3 films used for SEM, XRD, and Hall measurements was approximately 3, 3, and 1.1 μm, respectively. All film thickness was measured by the Alpha-Step IQ surface profiler.

Fabrication and characterization of LED devices: To prepare the LEDs, a small piece of n-type 4H-SiC substrate (Cree Inc., USA) was first cleaned with acetone followed by deionized (DI) water. The substrate was subsequently treated with O_2 plasma to make its surface hydrophilic for better wetting of the MoS_2 suspension during the film coating. The MoS_2 suspension was then carefully sprayed onto the SiC substrate for in situ oxidization of MoS_2 to $MoS_{2-x}O_x$. The thickness of the sprayed $MoS_{2-x}O_x$ film was approximately 3 μm. The oxide component structure of the $MoS_{2-x}O_x$ film was crystallized to form a MoS_2–MoO_3 film on a SiC substrate after the annealing process in 5 % H_2-diluted Ar gas at 450–500 °C for 1 h. Note, the MoS_2 crystal severely degraded when it was annealed above 500 °C in pure Ar.[22] The obtained n-SiC/p-MoS_2–MoO_3 heterojunction was used as the active layer in LEDs. The rear electrode of Ti(10 nm)/Au(120 nm) was coated onto the opposite side of the n-SiC substrate by electron-beam evaporation (Figure 1 d). The commercial ITO-coated glass was used as the front transparent electrode in the LED device. The final LED device had a configuration of Au/Ti/n-SiC/p-MoS_2–MoO_3/ITO/glass and was subsequently characterized under ambient conditions. The current-voltage (*I-V*) curve was measured by using Yokogawa GS610 source and measurement unit. The electroluminescence (EL) spectra were recorded using a PDS-1 photomultiplier tube detector connected to a monochromator.

Theoretical calculation: The calculation was performed using the planewave code Vienna ab initio simulation package (VASP).[23] Spin-polarized calculations using the projector augmented wave method with the Perdew-Burke-Ernzerhof functional (PAW-PBE)[24] were performed. A cutoff energy of 400 eV and $2\times2\times2$ mesh in *k*-space were adopted. A $3\times3\times3$ supercell was used and the structures were relaxed until the Hellmann-Feynman forces become less than 0.01 eV $Å^{-1}$. Since the lack of self-interaction corrections in normal DFT fails to reproduce electronic features of the highly delocalized defective states in d^0 oxides such as TiO_2 and MoO_3, the hybrid functionals (HSE06)[25] were used to calculate the defective states in the band gap. The calculated band gap of MoO_3 is 3.10 eV which is consistent with the experimental value of approximately 3.2 eV.[26]

Received: March 2, 2014
Revised: June 11, 2014
Published online: July 22, 2014

Keywords: electroluminescence · hybrid nanomaterials · light-emitting diodes · molybdenum · p-type doping

[1] a) X. Huang, Z. Zeng, H. Zhang, *Chem. Soc. Rev.* **2013**, *42*, 1934–1946; b) M. Chhowalla, H. S. Shin, G. Eda, L.-J. Li, K. P. Loh, H. Zhang, *Nat. Chem.* **2013**, *5*, 263–275; c) Q. H. Wang, K. Kalantar-Zadeh, A. Kis, J. N. Coleman, M. S. Strano, *Nat. Nanotechnol.* **2012**, *7*, 699–712.

[2] a) K. S. Novoselov, D. Jiang, F. Schedin, T. J. Booth, V. V. Khotkevich, S. V. Morozov, A. K. Geim, *Proc. Natl. Acad. Sci. USA* **2005**, *102*, 10451–10453; b) H. Li, G. Lu, Z. Yin, Q. He, H. Li, Q. Zhang, H. Zhang, *Small* **2012**, *8*, 682–686.

[3] J. N. Coleman, M. Lotya, A. O'Neill, S. D. Bergin, P. J. King, U. Khan, K. Young, A. Gaucher, S. De, R. J. Smith, I. V. Shvets, S. K. Arora, G. Stanton, H.-Y. Kim, K. Lee, G. T. Kim, G. S. Duesberg, T. Hallam, J. J. Boland, J. J. Wang, J. F. Donegan, J. C. Grunlan, G. Moriarty, A. Shmeliov, R. J. Nicholls, J. M. Perkins, E. M. Grieveson, K. Theuwissen, D. W. McComb, P. D. Nellist, V. Nicolosi, *Science* **2011**, *331*, 568–571.

[4] a) Z. Zeng, Z. Yin, X. Huang, H. Li, Q. He, G. Lu, F. Boey, H. Zhang, *Angew. Chem.* **2011**, *123*, 11289–11293; *Angew. Chem. Int. Ed.* **2011**, *50*, 11093–11097; b) G. Eda, H. Yamaguchi, D. Voiry, T. Fujita, M. Chen, M. Chhowalla, *Nano Lett.* **2011**, *11*, 5111–5116.

[5] a) Z. L. Y. Zhan, S. Najmaei, P. M. Ajayan, J. Lou, *Small* **2012**, *8*, 966–971; b) Y.-H. Lee, X.-Q. Zhang, W. Zhang, M.-T. Chang, C.-T. Lin, K.-D. Chang, Y.-C. Yu, J. T.-W. Wang, C.-S. Chang, L.-J. Li, T.-W. Lin, *Adv. Mater.* **2012**, *24*, 2320–2325.

[6] a) E. M. Hemamala, I. Karunadasa, Y. Sun, M. Majda, J. R. Long, C. J. Chang, *Science* **2012**, *335*, 698–702; b) T. F. Jaramillo, K. P. Jørgensen, J. Bonde, J. H. Nielsen, S. Horch, I. Chorkendorff, *Science* **2007**, *317*, 100–102.

[7] B. Radisavljevic, A. Radenovic, J. Brivio, V. Giacometti, A. Kis, *Nat. Nanotechnol.* **2011**, *6*, 147–150.

[8] a) A. N. P. Subhamoy Ghatak, A. Ghosh, *ACS Nano* **2011**, *5*, 7707 – 7712; b) See Ref. [7]; c) D. J. Late, B. Liu, H. S. S. R. Matte, V. P. Dravid, C. N. R. Rao, *ACS Nano* **2012**, *6*, 5635 – 5641.

[9] a) K. F. Mak, C. Lee, J. Hone, J. Shan, T. F. Heinz, *Phys. Rev. Lett.* **2010**, *105*, 136805; b) A. Splendiani, L. Sun, Y. Zhang, T. Li, J. Kim, C.-Y. Chim, G. Galli, F. Wang, *Nano Lett.* **2010**, *10*, 1271 – 1275.

[10] a) Z. Yin, H. Li, H. Li, L. Jiang, Y. Shi, Y. Sun, G. Lu, Q. Zhang, X. Chen, H. Zhang, *ACS Nano* **2012**, *6*, 74 – 80; b) H. S. Lee, S.-W. Min, Y.-G. Chang, M. K. Park, T. Nam, H. Kim, J. H. Kim, S. Ryu, S. Im, *Nano Lett.* **2012**, *12*, 3695 – 3700; c) Y. Ye, Z. Ye, M. Gharghi, H. Zhu, M. Zhao, X. Yin, X. Zhang, arXiv:1305.4235; d) O. Lopez-Sanchez, E. A. Llado, V. Koman, A. F. i Morral, A. Radenovic, A. Kis, arXiv:1403.2743; e) R.Cheng, D. Li, H. Zhou, C. Wang, A. Yin, S. Jiang, Y. Liu, Y. Chen, Y. Huang, X. Duan, arXiv:1403.3447.

[11] L. Britnell, R. V. Gorbachev, R. Jalil, B. D. Belle, F. Schedin, A. Mishchenko, T. Georgiou, M. I. Katsnelson, L. Eaves, S. V. Morozov, N. M. R. Peres, J. Leist, A. K. Geim, K. S. Novoselov, L. A. Ponomarenko, *Science* **2012**, *335*, 947 – 950.

[12] T. Georgiou, R. Jalil, B. D. Belle, L. Britnell, R. V. Gorbachev, S. V. Morozov, Y.-J. Kim, A. Gholinia, S. J. Haigh, O. Makarovsky, L. Eaves, L. A. Ponomarenko, A. K. Geim, K. S. Novoselov, A. Mishchenko, *Nat. Nanotechnol.* **2013**, *8*, 100 – 103.

[13] W. J. Yu, Z. Li, H. Zhou, Y. Chen, Y. Wang, Y. Huang, X. Duan, *Nat. Mater.* **2013**, *12*, 246 – 252.

[14] a) K. Chang, W. X. Chen, *ACS Nano* **2011**, *5*, 4720 – 4728; b) H. Hwang, H. Kim, J. Cho, *Nano Lett.* **2011**, *11*, 4826 – 4830.

[15] Y. Hou, A. B. Laursen, J. Zhang, G. Zhang, Y. Zhu, X. Wang, S. Dahl, I. Chorkendorff, *Angew. Chem.* **2013**, *125*, 3709 – 3713; *Angew. Chem. Int. Ed.* **2013**, *52*, 3621 – 3625.

[16] C. A. Papageorgopoulos, W. Jaegermann, *Surf. Sci.* **1995**, *338*, 83 – 93..

[17] F. Wypych, R. Schollhorn, *Chem. Commun.* **1992**, 1386 – 1388.

[18] A. Chithambararaj, A. C. Bose, *J. Alloys Compd.* **2011**, *509*, 8105 – 8110.

[19] a) M. A. Zimmler, J. Bao, I. Shalish, W. Yi, J. Yoon, V. Narayanamurti, F. Capasso, *Nanotechnology* **2007**, *18*, 235205; b) W. J. Yu, Y. Liu, H. Zhou, A. Yin, Z. Li, Y. Huang, X. Duan, *Nat. Nanotechnol.* **2013**, *8*, 952 – 958.

[20] C. Ataca, S. Ciraci, *J. Phys. Chem. C* **2011**, *115*, 13303 – 13311.

[21] M. T. Greiner, L. Chai, M. G. Helander, W.-M. Tang, Z.-H. Lu, *Adv. Funct. Mater.* **2012**, *22*, 4557 – 4568.

[22] K. K. Liu, W. J. Zhang, Y. H. Lee, Y. C. Lin, M. T. Chang, C. Su, C. S. Chang, H. Li, Y. M. Shi, H. Zhang, C. S. Lai, L. J. Li, *Nano Lett.* **2012**, *12*, 1538 – 1544.

[23] G. Kresse, J. Furthmüller, *Phys. Rev. B* **1996**, *54*, 11169 – 11186.

[24] J. P. Perdew, K. Burke, M. Ernzerhof, *Phys. Rev. Lett.* **1996**, *77*, 3865 – 3868.

[25] J. Heyd, G. E. Scuseria, M. Ernzerhof, *J. Chem. Phys.* **2003**, *118*, 8207 – 8215.

[26] D. O. Scanlon, G. W. Watson, D. J. Payne, G. R. Atkinson, R. G. Egdell, D. S. L. Law, *J. Phys. Chem. C* **2010**, *114*, 4636 – 4645.

[27] I. Popov, G. Seifert, D. Tománek, *Phys. Rev. Lett.* **2012**, *108*, 156802.

[28] S. Das, H. Y. Chen, A. V. Penumatcha, J. Appenzeller, *Nano Lett.* **2013**, *13*, 100 – 105.

[29] J. R. Chen, P. M. Odenthal, A. G. Swartz, G. C. Floyd, H. Wen, K. Y. Luo, R. K. Kawakami, *Nano Lett.* **2013**, *13*, 3106 – 3110.

[30] A. Dankert, L. Langouche, M. V. Kamalakar, S. P. Dash, *ACS Nano* **2014**, *8*, 476 – 482.

[31] a) Z. Tang, P. D. Ye, D. Lee, C. R. Wie, *Microelectron. Reliab.* **2007**, *47*, 2082 – 2087; b) J. S. Kim, J. H. Park, J. H. Lee, J. Jo, D. Kim, K. Cho, *Appl. Phys. Lett.* **2007**, *91*, 112111; c) J. H. Zhao, K. Sheng, R. C. Lebron-Velilla, *Int. J. High Speed Electron. Syst.* **2005**, *15*, 821; d) M. S. Choi, G. H. Lee, Y. J. Yu, D. Y. Lee, S. H. Lee, P. Kim, J. Hone, W. J. Yoo, *Nat. Commun.* **2013**, *4*, 1624; e) V. Shrotriya, G. Li, Y. Yao, C. W. Chu, Y. Yang, *Appl. Phys. Lett.* **2006**, *88*, 073508.

